Journal of Power Sources 273 (2015) 351–359

Contents lists available at ScienceDirect

Journal of Power Sources

journal homepage: www.elsevier.com/locate/jpowsour

Entropy change characteristics of $LiMn_{0.67}Fe_{0.33}PO_4$ and $Li_4Ti_5O_{12}$ electrode materials

K. Jalkanen, K. Vuorilehto*

Department of Chemistry, School of Chemical Technology, Aalto University, P.O. Box 16100, 00076 Aalto, Finland

HIGHLIGHTS

- Entropy change of $LiMn_{0.67}Fe_{0.33}PO_4$ follows the Fe and Mn redox reaction regions.
- Substituting Mn for Fe changes the Fe redox couple entropy change profile.
- The change is suggested to be due to changes in Fe redox couple reaction mechanism.
- $Li_4Ti_5O_{12}$ shows a typical two-phase reaction entropy change except for near 0% SOC.
- The reversible heat generation of a $LiMn_{0.67}Fe_{0.33}PO_4/Li_4Ti_5O_{12}$ cell is simulated.

GRAPHICAL ABSTRACT

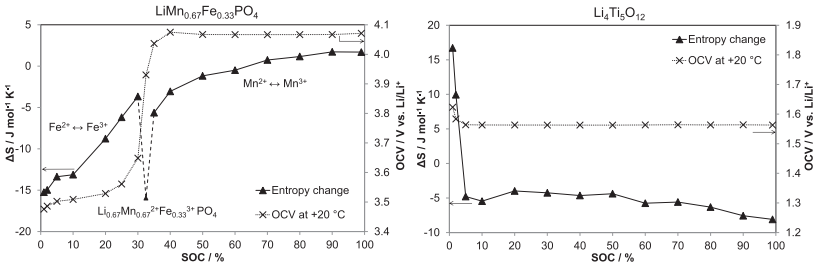

ARTICLE INFO

Article history:
Received 8 July 2014
Received in revised form
31 August 2014
Accepted 12 September 2014
Available online 22 September 2014

Keywords:
Lithium-ion cell
Entropy change
Reversible heat generation
Lithium manganese iron phosphate
Lithium titanate

ABSTRACT

The combination of $LiMn_{0.67}Fe_{0.33}PO_4$ positive and $Li_4Ti_5O_{12}$ negative electrode is studied in terms of its entropy change behavior, which affects the reversible heat generation of a lithium-ion cell. This electrode combination is especially interesting for large applications, as it is proposed to be a very safe choice having still an adequate energy density. The entropy change of $LiMn_{0.67}Fe_{0.33}PO_4$ and $Li_4Ti_5O_{12}$ electrode materials is measured at different states of charge using a potentiometric method. The results are compared with conventional electrode materials, $LiFePO_4$ and artificial graphite. The entropy change of $LiMn_{0.67}Fe_{0.33}PO_4$ is found to follow the distinct plateaus of Fe^{2+}/Fe^{3+} and Mn^{2+}/Mn^{3+} redox couples and to be clearly different from $LiFePO_4$. This difference is suggested to be due to single-phase solid solution regions, originating from effects of substituting Mn for Fe. For $Li_4Ti_5O_{12}$, mostly a constant entropy change typical for a two-phase reaction is observed, except for the region near 0% state of charge. The data from individual electrodes is used to simulate and compare the entropy change behavior and thus the reversible heat generation rate of different electrode combinations.

© 2014 Elsevier B.V. All rights reserved.

1. Introduction

Lithium-ion batteries have found applications in large systems, like electric vehicles and energy storage applications, which have emphasized the matters of safety, cycle life and cost. Although many factors affect the battery pack behavior, the cell level safety is always fundamental and it depends on the electrode materials' properties.

Traditionally, lithium-ion batteries have used lithium cobalt oxide $LiCoO_2$ (LCO) at the positive electrode and graphite at the negative electrode. Severe safety problems and the high cost and toxicity of cobalt restrict the use of LCO in large batteries. On the

* Corresponding author.
E-mail address: kai.vuorilehto@helsinki.fi (K. Vuorilehto).

http://dx.doi.org/10.1016/j.jpowsour.2014.09.091
0378-7753/© 2014 Elsevier B.V. All rights reserved.

negative electrode side, the potential of lithium intercalated graphite (0.1–0.2 V vs. Li/Li^+) is outside the electrolyte stability window, causing the formation of a passivating solid electrolyte interface (SEI) layer on the graphite electrode surface. The instability of this SEI-layer and the relatively large, 10% volume change of graphite lattice during lithium intercalation/deintercalation restrict the cycle life and stability of graphite based cells. In addition, the low potential of graphite negative electrode introduces a risk of lithium plating and a consequential short circuit, especially when charged with higher currents and at cold temperatures.

To overcome problems at the graphite negative electrode, lithium titanate $Li_4Ti_5O_{12}$ (LTO) has been proposed as a promising alternative [1–4]. LTO is a very safe material: its equilibrium potential lies relatively high, at 1.55 V vs. Li/Li^+ [1], preventing SEI-layer formation and the risk of lithium plating [5]. This enables the safe use of high charging currents and charging at cold temperatures, but also decreases the obtainable cell voltage. The cycle life of an LTO electrode is excellent as it is a so called “zero-strain material”, experiencing almost no change in lattice dimensions upon lithium intercalation/deintercalation [1,6–8].

On the positive electrode side, LCO material has been replaced with lithium iron phosphate $LiFePO_4$ (LFP) in many applications. LFP is a very safe material due to its stable olivine structure; furthermore, it is non-toxic and inexpensive. On the other hand, LFP shows poor electric and ionic conductivity, but its electrochemical performance has been successfully improved by coating the particles with conductive carbon layer and by minimizing the particle size [9,10]. However the equilibrium potential of LFP is relatively low, 3.4 V vs. Li/Li^+ [11], when compared to LCO. Thus when combining LFP and LTO, the theoretical cell voltage remains low, only at 1.85 V. This decreases the energy density of an LFP/LTO cell substantially.

For increasing the cell voltage and energy density without compromising safety, combining LTO with other olivine structured phosphates than LFP seems to be an interesting choice. One promising candidate is lithium manganese phosphate $LiMnPO_4$ (LMP), which has a high equilibrium potential of 4.1 V vs. Li/Li^+ [11]. However, the performance of pure LMP as electrode material has some serious limitations: very poor electronic conductivity (even worse than that of LFP) [12–14], structural instability due to lattice distortion around Mn^{3+} caused by the strong electron–lattice interaction (Jahn–Teller effect), and the consequential lattice mismatch between $LiMnPO_4$ and $MnPO_4$ [14–16]. These factors result in a low rate capability and large polarization [12,13], and consequently not all the theoretical capacity of LMP can be utilized.

A compromise is to combine LMP and LFP by creating a mixed system of $LiMn_yFe_{1-y}PO_4$ (LMFP), which is a solid solution between the two olivine compounds $LiMnPO_4$ and $LiFePO_4$ [11,14], consisting of naturally abundant, non-toxic elements. LMFP shows two distinct voltage plateaus: one for the Fe^{2+}/Fe^{3+} and one for the Mn^{2+}/Mn^{3+} redox couple, and the high potential of Mn^{2+}/Mn^{3+} raises the material's average potential compared to LFP. Thus by increasing the Mn content, higher cell voltages and consequently also higher energy densities can be obtained. However, the material's electrochemical performance deteriorates with the increasing Mn content [12,14,17]. LMFP materials have been reported to be unstable and not able to deliver their full capacity at higher Mn contents than $y > 0.8$ [11,14,18], due to having the limitations of pure LMP. Typically, Mn contents of $0.6 < y < 0.8$ are suggested to be used [14,17–21] in order to maximize the energy density. In terms of thermal safety, LMFP, being a solid-solution of two olivine compounds, is expected to resemble LFP. However, there is some discrepancy in results. LMP has been suggested to be thermally unstable in the delithiated ($MnPO_4$) form [22–24], which would put the thermal stability of LMFP in question. On the other hand, other studies have shown a greatly improved thermal stability of LMFP in comparison to layered oxide cathode materials [20,25], or even found no evidence of lower thermal stability of LMFP or LMP compared to LFP [26]. Despite the high potential of Mn^{2+}/Mn^{3+} redox couple, the reactivity of LMFP with standard electrolyte solutions has been predicted to be relatively low, because phosphates are less surface active with electrolyte species than layered oxide high-voltage cathode materials [19,27]. Still, film formation on LMFP electrode surface has been demonstrated [28]. The combination of LMFP and LTO seems to be a very promising alternative for a next generation lithium-ion battery and the combination has been presented in literature [19,21]. LMFP/LTO cell could give a voltage of 2.5 V, when operating at SOCs at the higher potential Mn plateau in LMFP.

In addition to the performance characteristics, electrode materials affect the cell's thermal behavior. As new lithium-ion battery applications often require large battery packs, heat control and cooling systems become more critical. For designing a suitable cooling system, the amount of heat that is generated by an individual cell has to be known. The heat generation of a lithium-ion cell and its dependence on the positive and negative electrode materials are discussed here next. More detailed discussion can be found in a previous work [29] and in literature elsewhere [30,31].

The total heat generation rate Q_{total} of a lithium-ion cell consists of irreversible and reversible parts as follows [30–32]:

$$Q_{total} = Q_{irreversible} + Q_{reversible} = -I^2R_i + T\Delta S\frac{I}{nF} \quad (1)$$

where I is the current value (discharge current is here determined to be positive), R_i is the cell internal resistance and ΔS is the entropy change. Negative Q implies an exothermic cell reaction and heat transfer from the cell to the surroundings. On the contrary, positive Q indicates that heat is absorbed to the cell. $Q_{irreversible}$ is always negative and associated with heat production whereas the sign of $Q_{reversible}$ depends on the sign of ΔS and current direction. The contributions of $Q_{irreversible}$ and $Q_{reversible}$ define the sign and magnitude of Q_{total} that is the amount of heat the cell is either evolving or absorbing.

The entropy change is a measure of the ordering or disordering of lithium-ions in the electrode material lattices. Increased order results in a negative entropy change as charge is passed through the cell, whereas a positive entropy change implies increased disorder. The overall cell entropy change consists of the positive and negative electrode contributions. In the cell discharge direction, the corresponding entropy changes are for reduction at the positive and oxidation at the negative electrode. The measured values in this work are for the reduction reaction. Thus the entropy change values measured for negative electrodes have to be reversed in sign to give the entropy change for oxidation. This gives for the full cell discharge direction entropy change:

$$\begin{aligned}\Delta S_{\text{full cell, discharge}} &= \Delta S_{\text{positive electrode, reduction}} \\ &\quad + \Delta S_{\text{negative electrode,oxidation}} \\ &= \Delta S_{\text{positive electrode, reduction}} \\ &\quad - \Delta S_{\text{negative electrode, reduction}}\end{aligned} \quad (2)$$

Entropy change can be determined potentiometrically or calorimetrically. In this work, the potentiometric method was used, where entropy change is related to the cell open circuit voltage (OCV) through the Gibbs free energy change [33]. This is expressed as:

$$OCV = -\frac{\Delta H}{nF} + \frac{T\Delta S}{nF} \quad (3)$$

where $n = 1$ for a lithium-ion cell. When OCV is recorded at different temperatures, the entropy change can be calculated from the slope as follows:

$$\Delta S = F\frac{\partial(\mathrm{OCV})}{\partial T} \quad (4)$$

In this work, the entropy change behavior at different states of charge was measured for LMFP ($LiMn_{0.67}Fe_{0.33}PO_4$) and LTO electrode materials. To our knowledge, the entropy change of LTO materials has been studied only a little [32,34] and the entropy change of LMFP materials only by Dodd [35], who performed thermodynamic measurements on $LiMn_{0.2}Fe_{0.8}PO_4$. However, to our knowledge, this is the first time that an LMFP material with a high Mn content is studied in terms of the entropy change. Moreover, although the LMFP/LTO combination has been studied for its electrochemical performance, its thermal characteristics have not been highlighted. As stated, to be able to exactly determine the cell level heat generation and the battery's thermal behavior, the entropy change behavior of the positive and negative electrode materials has to be taken into account. It is also important to compare the different chemistry combinations in order to find the beneficial and also the unfavorable pairings of positive and negative electrodes in terms of the cell's net entropy change and thus the reversible heat generation rate. The entropy change measurements were performed here potentiometrically using half-cells with a metallic lithium counter electrode. A confirming experiment was done with an LMFP/LTO full test cell. The origins of the entropy change characteristics are discussed and the results are compared with our previous study of LFP and artificial graphite [29]. The entropy change behavior of LMFP is observed to significantly differ from LFP. LTO material shows an entropy change behavior typical for a two-phase reaction, except for the near to 0% SOC composition. In addition, the effect of combining different positive and negative electrodes on the full cell net entropy change and consequently on the cell's thermal behavior is simulated.

2. Experimental

2.1. Electrode slurry preparation

Electrode slurries were prepared by first dissolving polyvinylidene fluoride (PVDF) (Solef 5130) in *N*-methylpyrrolidone (Ashland) and then adding carbon black (Timcal SuperC 65) and the active material powder (LMFP or LTO). The mixing was done with a dispergator mixer (IKA T25). The tested electrode materials were carbon coated C-$LiMn_{0.67}Fe_{0.33}PO_4$ (Clariant, Germany) and $Li_4Ti_5O_{12}$ (T1, Clariant, Germany). LMFP slurry composition was 93.0 wt% C-LMFP, 4.7 wt% PVDF and 2.3 wt% carbon black, and the LTO slurry composition 94.4 wt% LTO, 2.8 wt% PVDF and 2.8 wt% carbon black. The mixed slurries were applied on aluminum foil with doctor blade technique and first dried at room temperature overnight and then at +60 °C for 2 h. Samples of 18 mm diameter were cut from the electrode sheets and calendared with a 2.75 t cm^{-2} pressure.

2.2. Test cell assembly

Electrochemical test cells (EL-Cell, Germany) of 18 mm diameter were used to test the electrode materials. The calendared electrode samples and all cell parts were first dried in vacuum at +100 °C for 24 h. The cells were then transferred in vacuum to an argon-filled glove box, where they were assembled. A 0.65 mm thick glass fiber separator of 18 mm diameter (provided by EL-Cell) was used. For half-cell experiments the counter electrode was metallic lithium (Sigma–Aldrich, thickness 0.75 mm, 99.9% trace metals basis). The electrolyte solution was received from European Batteries Ltd. and it consisted of 1 M $LiPF_6$ dissolved in a quaternary mixture of ethylene carbonate (EC) and other common organic carbonates.

2.3. Electrochemical measurements

Electrochemical testing was performed using a Maccor battery cycler (Maccor 4300, USA). The cut-off voltages for cycling are presented in Table 1. To be consistent with a full lithium-ion cell, the lithiation of LTO in the LTO/lithium half-cells is referred to as charging. The nominal capacities were calculated based on the active material's mass in each sample; in the full LMFP/LTO-cell the LMFP electrode limited the nominal capacity. Before the potentiometric measurements, the actual capacity of the cells was determined with a slow charge–discharge cycle at 0.03C rate.

The potentiometric measurements were carried out in a temperature chamber (ESPEC, model BTZ-175E), using active air circulation for constant temperature condition. The SOC of the tested cell was adjusted at +20 °C using 0.1C current. The cell was defined to be at 100% SOC after a constant current charge followed by a constant voltage charge at the cut-off voltage until the current was reduced to 0.03C. Similarly, a constant current discharge followed by a constant voltage discharge until current reduced to 0.03C was defined as 0% SOC. When the cell's SOC was adjusted, it was left to stabilize for 20 h at +20 °C. After stabilization, the chamber temperature was first decreased to 0 °C for 2 h and then increased by 10 °C intervals and 1.5 h stabilization time until +30 °C was reached. Finally the temperature was decreased back to +20 °C for 2 h. The cell's OCV was measured and registered at 20 s intervals and the average value of the recorded OCVs during the last 30 min of each temperature was taken as the result. The same test regime was repeated at different SOCs.

The entropy change in half-cells was measured against metallic lithium. It is assumed, that neither the lithium counter electrode composition nor the chemical environment of the lithium atoms changes during the cell reaction and thus the entropy change characteristics as function of SOC are attributed to the changes in LMFP and LTO electrode materials [32,36,37]. All the half-cell entropy change values are presented for the reduction reaction direction in this work.

3. Results and discussion

3.1. Potential profiles of LMFP and LTO

The LMFP and LTO half-cell voltages measured at 0.03C rate prior to the potentiometric experiments are shown in Fig. 1. For comparison, corresponding data from a previous study for LFP and graphite [29] is also shown.

As shown in Fig. 1a, the LMFP electrode potential consists of two regions: one at lower 3.5 V vs. Li/Li^+ potential corresponding to the Fe^{2+}/Fe^{3+} redox couple and one at higher 4.05 V vs. Li/Li^+ potential corresponding to the Mn^{2+}/Mn^{3+} redox couple. It is seen that the

Table 1
Cut-off voltages for cycling.

	Charge cut-off voltage/V	Discharge cut-off voltage/V
LMFP half-cell (LMFP vs. lithium)	4.25 (vs. Li/Li^+)	2.7 (vs. Li/Li^+)
LTO half-cell (LTO vs. lithium)	1.2 (vs. Li/Li^+)	1.9 (vs. Li/Li^+)
LMFP vs. LTO	2.7	1.2

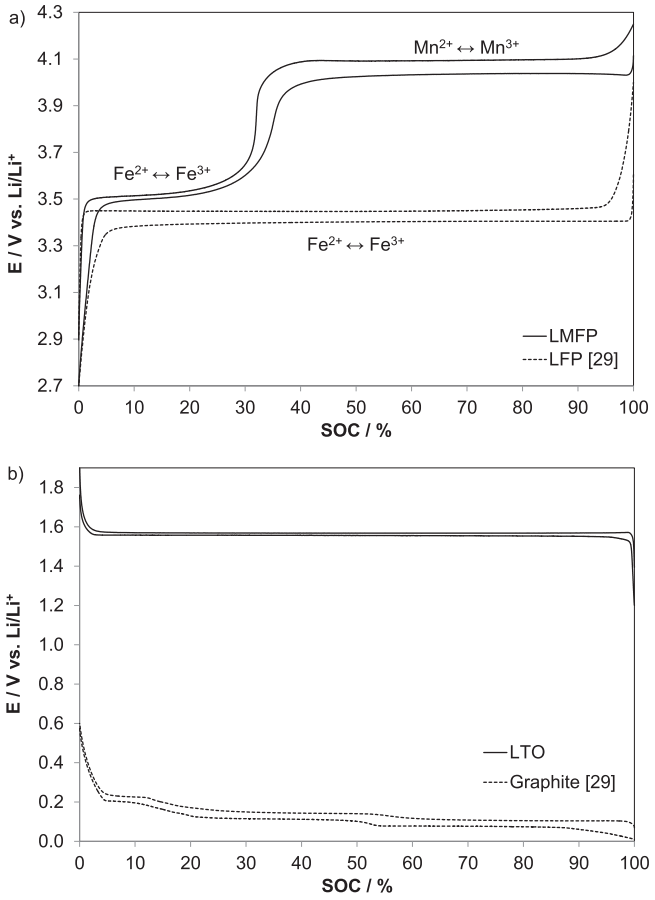

Fig. 1. Half-cell voltage (vs. metallic lithium) as a function of SOC at 0.03C constant current. (a) LMFP and LFP [29]; (b) LTO and graphite. [29].

capacity ratio of these potential regions is equivalent to the Fe:Mn ratio (1:2) in the LMFP material. The potential values differ slightly from the theoretical ones, 3.4 V for Fe^{2+}/Fe^{3+} and 4.1 V for Mn^{2+}/Mn^{3+}. The substitution of Mn for Fe is known to raise the Fe^{2+}/Fe^{3+} redox couple potential and lower the Mn^{2+}/Mn^{3+} redox couple potential [38–40]. For LMFP materials with different Fe:Mn ratios, a systematic upward shift of both redox potentials with increasing Mn content has been observed [38]. This has been reported to result from strong Mn–O–Fe coupling interaction (*superexchange*) [11,40,41], and from changes in the covalency of the Fe/Mn–O bond mainly due to changes in the lattice parameters and Fe/Mn–O bond lengths [38,41].

If the potential profile of LMFP is investigated more in detail, it can be observed that the Fe^{2+}/Fe^{3+} region actually is s-shaped and the Mn^{2+}/Mn^{3+} region flat. This is inconsistent with the Fe^{2+}/Fe^{3+} couple potential behavior in LFP, where the Fe^{2+}/Fe^{3+} redox reaction proceeds as a two-phase reaction between $LiFePO_4$ and $FePO_4$ phases [11]. The reaction mechanism in the Fe^{2+}/Fe^{3+} region of LMFP has been discussed to be different. Yamada et al. [18,40] first reported that a single-phase reaction region of the Fe^{2+}/Fe^{3+} redox couple appears in LMFP materials. As lithium is extracted from the material, a partial conversion of the Fe^{2+}/Fe^{3+} redox reaction from a two-phase to a single-phase solid solution reaction was proposed. For Mn contents of $y > 0.60$, the Fe^{2+}/Fe^{3+} reaction was reported to proceed via the single-phase mechanism, described as $Li_xMn_y^{2+}Fe_{1-y}^{a+}PO_4$ ($1 \geq x > y$ and $2 \leq a \leq 3$). The Mn^{2+}/Mn^{3+} redox reaction was claimed to proceed as a two-phase reaction between $Li_yMn_y^{2+}Fe_{1-y}^{3+}PO_4$ and $Mn_y^{3+}Fe_{1-y}^{3+}PO_4$ phases for the whole Mn^{2+}/Mn^{3+} region.

Partly contradictory results and phase diagrams have however been presented. Bramnik et al. [42] proposed a two-phase mechanism for the Fe^{2+}/Fe^{3+} redox couple in $Li_xMn_{0.6}Fe_{0.4}PO_4$, and found a single-phase region only in the intermediate compositions (approximately $0.55 < x < 0.7$), where the Fe^{2+}/Fe^{3+} redox reaction is changed to the Mn^{2+}/Mn^{3+} redox reaction. Similar observations were presented by Nam et al. [43] for $Li_xMn_{0.5}Fe_{0.5}PO_4$ suggesting that the Fe^{2+}/Fe^{3+} and Mn^{2+}/Mn^{3+} redox reactions would proceed simultaneously during a narrow single-phase region ($0.4 \leq x \leq 0.5$). Also Malik et al. [44] calculated a narrower single-phase region for the Fe^{2+}/Fe^{3+} redox couple, and found the single-phase region to be extended to the Mn^{2+}/Mn^{3+} region. Roberts et al. [45] suggested two-phase mechanisms only at the extremes of the lithium concentrations and a single-phase mechanism in the intermediate region, and Molenda et al. [46,47] proposed a single-phase mechanism at all lithium concentrations ($1 \geq x \geq 0$) for varying Mn contents. Lately Hashambhoy et al. [48] reported phase behavior results for $LiMn_{0.5}Fe_{0.5}PO_4$ consistent with the studies of Yamada et al. [18,40].

Although various phase diagrams have been proposed, there seems to be a consistency of the appearance of a single-phase region close to the transition between Fe^{2+}/Fe^{3+} and Mn^{2+}/Mn^{3+} redox reactions ($x = y$ in $Li_xMn_yFe_{1-y}PO_4$). The single-phase behavior has been attributed to the effect of Mn^{2+}, which dilutes the interactions responsible for the phase separation and thus the two-phase reaction behavior of Fe^{2+}/Fe^{3+} in LFP [40,44]. The appearance of single-phase regions in metal phosphates is not only affected by temperature [44,49,50], but has also been reported to depend on particle size [49,50] and the means of lithium extraction (chemical vs. electrochemical) [46,47]. These factors probably partly account for the contradictory phase diagram results.

In Fig. 1a, the gap between the charge and discharge voltages is much smaller in the Fe^{2+}/Fe^{3+} region than in the Mn^{2+}/Mn^{3+} region, that is, the Fe^{2+}/Fe^{3+} region shows less polarization. In addition, the polarization in the Fe^{2+}/Fe^{3+} region of LMFP is actually also observed to be smaller than in pure LFP. However, due to differences between the electrodes, for example in active material particle size, the comparison cannot be made with full accuracy, although the test cell construction was identical. The Fe^{2+}/Fe^{3+} and Mn^{2+}/Mn^{3+} redox couples have been demonstrated to show opposite kinetic behavior as function of increasing Mn content [38,44], resulting in reduced polarization in the Fe^{2+}/Fe^{3+} redox region and increased polarization in the Mn^{2+}/Mn^{3+} redox region.

In Fig. 1b, the LTO potential shows a flat plateau at 1.56 V vs. Li/Li^+. This corresponds to the two-phase reaction between the end-compositions of $Li_4Ti_5O_{12}$ spinel (0% SOC) and $Li_7Ti_5O_{12}$ rock salt (100% SOC) [1,7,8]. The additional lithium inserted to form the rock salt $Li_7Ti_5O_{12}$ occupies different positions than the lithium in the spinel $Li_4Ti_5O_{12}$ structure [1,8]. The existence of a solid-solution region in LTO has been a controversial issue. Scharner et al. [8] have proposed a solid-solution behavior inside the SOC range of 0–3% in the spinel $Li_4Ti_5O_{12}$, after which insertion of lithium-ions creates a two-phase region ($Li_4Ti_5O_{12}/Li_7Ti_5O_{12}$). Wagemaker et al. [51] suggested that the two-phase system would actually be unstable above 100 K temperatures and relax through lithium-ion diffusion to a single-phase solid-solution composition over the whole SOC range, when given time to reach equilibrium. However, when current is applied and especially at higher current rates the LTO electrode does not reach equilibrium and relaxation to a single-phase composition has not been observed [51,52]. In this work, the sloping potential between near 0% SOC and the sharp transition point at approximately 3% SOC observed in Fig. 1b indicate a solid-solution behavior at the applied very slow 0.03C current rate inside the 0–3% SOC range.

Compared to graphite, LTO has a very flat potential curve with less polarization. This results in smaller variation of the cell voltage

as function of the SOC and also in reduced voltage losses. However, the overall cell voltage is clearly lowered when LTO is used instead of graphite.

3.2. Entropy change behavior of half-cells

To calculate the entropy change values, the average value of the recorded OCVs for the last 30 min of each measurement temperature (0–30 °C) was taken and the OCV vs. temperature was plotted for every SOC. An example of the potentiometric measurements and the corresponding OCVs as function of temperature is shown in Fig. 2. The entropy change was obtained according to Eq. (4) by calculating it from the slope of the OCV vs. temperature -plot. The calculated entropy change values for LMFP are presented in Fig. 3a and for LTO in Fig. 4a. In addition, the OCV value taken from the +20 °C measurement is provided for each SOC in the figures. The corresponding measurements for LFP (Fig. 3b) and graphite (Fig. 4b) materials from a previous work [29] are presented for comparison.

In pure LFP, the Fe^{2+}/Fe^{3+} redox reaction proceeds via a two-phase mechanism, where only the ratio of phases filled with lithium ($LiFePO_4$) and empty of lithium ($FePO_4$) changes, but the phase compositions and the degree of ordering remain the same as more lithium-ions are added/extracted. This is seen as a nearly constant entropy change of LFP in Fig. 3b. In the Mn^{2+}/Mn^{3+} redox region of LMFP, a rather similar behavior to pure LFP is observed, showing a nearly constant entropy change value especially inside 50–100% SOC, further away from the Fe–Mn transition region. According to Yamada et al. [18,40], the Mn^{2+}/Mn^{3+} redox region proceeds entirely as a two-phase reaction between the phases filled with lithium ($Li_{0.67}Fe_{0.33}Mn_{0.67}PO_4$) and empty of lithium ($Fe_{0.33}Mn_{0.67}PO_4$). Particularly, when compared to LFP [29,32,35,50], it is suggested that the entropy change behavior of Mn^{2+}/Mn^{3+} redox reaction in LMFP indicates two-phase behavior, at least above 50% SOC. Slightly sloping entropy change profile as function of SOC is observed for the Mn region. This trend has been observed for LFP [29,35], too. For some LFP materials, existence of single-phase regions near the end compositions has been suggested [50]. These regions have been proposed to result in sharp changes and a sloping profile in entropy change measurements [35,50]. Thus the more sloping entropy change profile near the Fe–Mn transition could originate from a single-phase behavior, extending to the Mn^{2+}/Mn^{3+} region.

In the Fe^{2+}/Fe^{3+} redox region and during the Fe–Mn transition of LMFP, however, the entropy change behavior is distinctly different from pure LFP and from typical two-phase reaction behavior. The entropy change is negative in sign throughout the Fe region, and decreases to more negative values as more lithium-ions are added to the structure (decreasing SOC). The +20 °C OCV values also show a clearly sloping profile inside 0–35% SOC. Also a sudden, sharp peak of negative entropy change is observed at SOC = 32.5%, where the OCV is very steeply changing, too. However, the recorded OCV vs. time at SOC = 32.5% showed an unstable behavior of continuous downward drift. Thus the entropy change result can only be taken as an approximate value and is plotted with dashed line in Fig. 3a. This observation will be discussed more in detail in Section 3.3.

According to Yamada et al. [18,40], in the LMFP material studied here (Mn content $y = 0.67$), the Fe^{2+}/Fe^{3+} redox reaction would

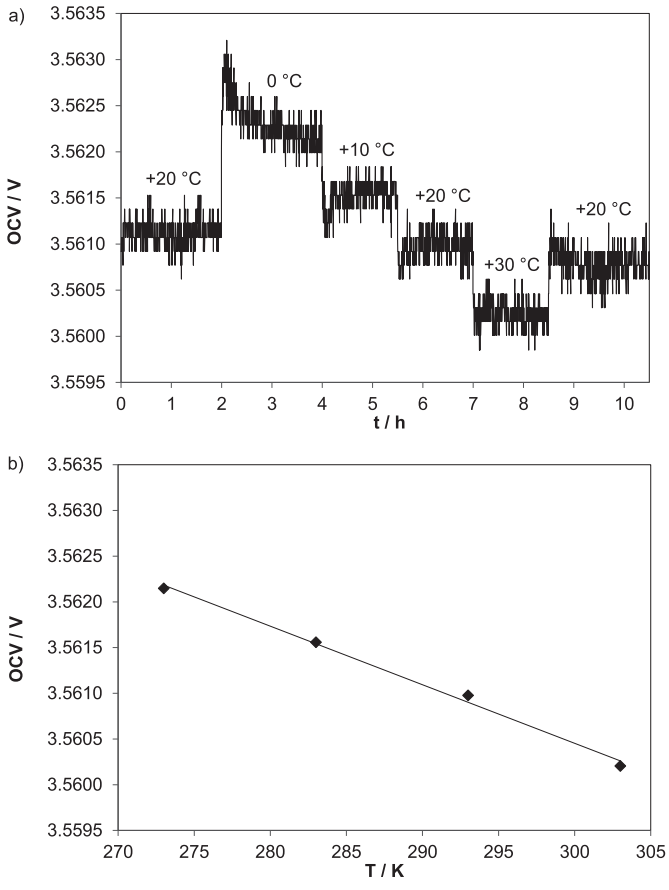

Fig. 2. (a) Potentiometric measurement (OCV vs. time); (b) the corresponding linear fitting (OCV vs. temperature, $R^2 = 0.995$) for LMFP half-cell at 25% SOC.

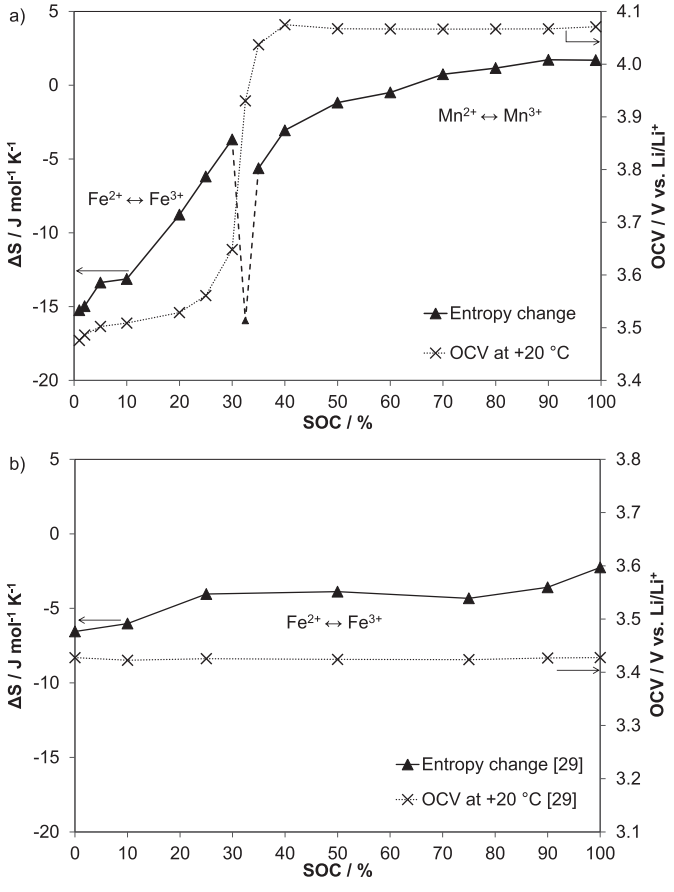

Fig. 3. Entropy change and OCV at +20 °C for the (a) LMFP; (b) LFP [29] half-cell.

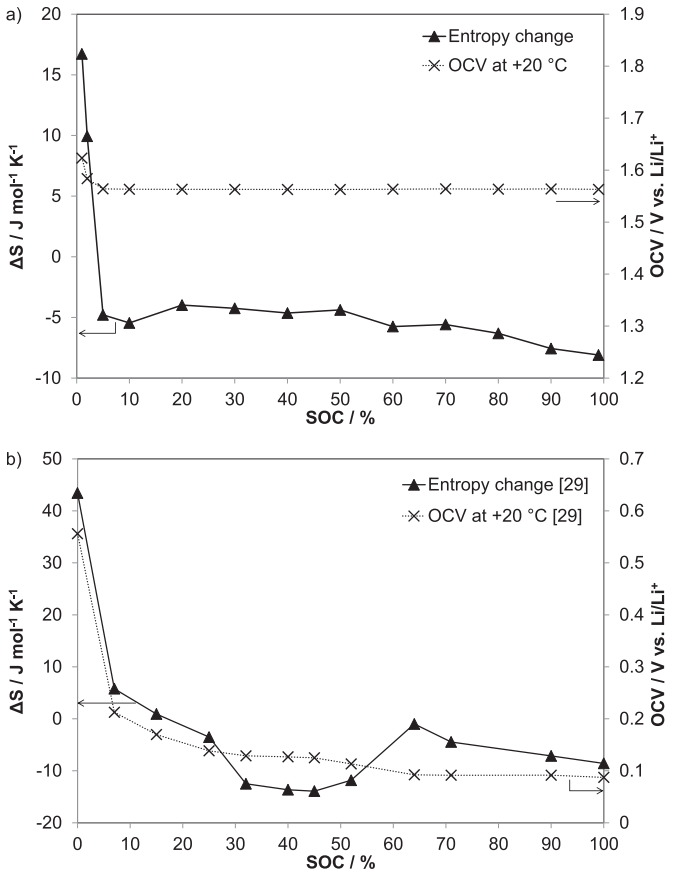

Fig. 4. Entropy change and OCV at +20 °C for the (a) LTO; (b) graphite [29] half-cell.

proceed entirely as a single-phase reaction having the composition of $Li_x(Mn^{2+}_{0.67}Fe^{a+}_{0.33})PO_4$ ($1 \geq x \geq 0.67$, $2 \leq a \leq 3$). This could explain the distinct, sloping behavior of the Fe^{2+}/Fe^{3+} region entropy change. As the SOC is decreased towards 0% SOC, the single-phase $Li_x(Mn^{2+}_{0.67}Fe^{a+}_{0.33})PO_4$ would show more negative entropy change values implying increased ordering as the composition approaches $LiMn^{2+}_{0.67}Fe^{2+}_{0.33}PO_4$ structure with all lithium sites filled.

The appearance of a sharp peak in the entropy change at 32.5% SOC is attributed to the Fe–Mn transition. For this region, single-phase behavior has been proposed in the literature [18,40,42–48] and the sharp entropy change supports this. The negative value of the peak implies a sudden ordering in the lattice. If the results of Yamada et al. [18,40] are again considered, the sharp peak would be due to the state where the two-phase Mn^{2+}/Mn^{3+} region is in its end composition, $Li_{0.67}Mn^{2+}_{0.67}Fe^{3+}_{0.33}PO_4$, and the addition of lithium-ions leads to the solid-solution region formation. This particular composition is speculated here to show a high degree of ordering, similar to a completely full or empty lattice.

The entropy change behavior measured by Dodd [35] for an LMFP material with a lower Mn content $y = 0.2$ (in this study $y = 0.67$) is for the most part in line with the results presented here, as the different Mn contents are taken into account. The Mn^{2+}/Mn^{3+} region in the measurement by Dodd is more difficult to interpret, as it is much narrower due to the lower Mn content. However, positive entropy change values were observed. If the phase diagrams proposed by Yamada et al. [18,40] are considered, Mn content of $y = 0.2$ should result in a division of the Fe^{2+}/Fe^{3+} region to two-phase and single-phase areas. Dodd measured a somewhat sloping profile for the Fe^{2+}/Fe^{3+} region and proposed a possible single-phase region, observed as a sloping entropy change profile, only in the intermediate SOCs of the Fe^{2+}/Fe^{3+} region and not reaching to the Fe–Mn transition region. Near the Fe–Mn transition, a sharp change in the entropy change profile was reported, which confirms our results. In addition, Dodd observed sharp spikes near 0% and 100% SOC, which were attributed to single-phase regions. This is different from the results obtained here, but could be explained again by the solid solution dependence on particle size and also on the Mn content.

When the entropy change behavior of Fe^{2+}/Fe^{3+} region in LMFP is compared to pure LFP, there is a clear difference in the entropy change behavior, caused by the partial substitution of Mn for Fe. Further studies are needed to conclude whether this is due to a single-phase reaction over the entire Fe^{2+}/Fe^{3+} redox reaction or just near the Fe–Mn transition, or if there is some other factor inducing the different entropy change behavior. Measurements with various Mn contents and concurrent phase diagram studies are needed to be able to unambiguously tell the effect of reaction mechanism on the entropy change behavior.

It is shown in Fig. 4a that the LTO entropy change remains constant in the SOC range of 5–100%, being only slightly negative. This is typical behavior for a two-phase reaction. Compared to graphite (Fig. 4b), the entropy change of LTO is closer to zero, and there is no staging phenomenon of multiple phases.

At SOCs smaller than 5%, the entropy change of LTO shows clearly positive values and a sloping profile. In addition, the +20 °C OCV values inside this region are higher when compared to the constant profile inside 5–100% SOC. We suggest that the distinct entropy change behavior near 0% SOC could be related to a single-phase solid-solution region, proposed by Scharner et al. [8] to exist at 0–3% SOC. At 5% and 10% SOC, the OCV vs. temperature curves showed peculiar hysteresis, which will be discussed later in Section 3.3.

The positive peak in entropy change close to 0% SOC implies increased disorder, when lithium is inserted to the LTO lattice (increasing SOC in Fig. 4a). Similar behavior is observed for graphite, where the dilute stage-1 of random intercalation without two-phase region is seen as positive entropy change peak inside 0–10% SOC range [29,36,37,53]. An empty lattice can be considered to be very ordered, and adding a few lithium-ions creates clearly a more disordered state [53,54]. Here the $Li_4Ti_5O_{12}$ spinel structure is considered as an ordered state, as the added lithium-ions are inserted in different sites.

Viswanathan et al. [32] and Lu et al. [34] have studied the entropy change of LTO. Viswanathan et al. [32] measured the entropy change potentiometrically, whereas Lu et al. [34] used a calorimetric method. Compared to the results presented here, they have measured a very identical trend of the entropy change as function of the SOC, showing a positive peak near 0% SOC and being almost constant and slightly negative at higher SOCs for the reduction reaction direction. However, Lu et al. [34] measured a sharp negative peak in the entropy change near 100% SOC. It is to be noticed that they cycled the LTO half-cell to a very low potential, 0.2 V vs. Li/Li^+, which could have caused side reactions, as the potential is outside the electrolyte stability window. Voltage variations below 1.0 V vs. Li/Li^+ and signs of a new phase formation were observed in their study. In this study, the cycling potential range was restricted to 1.2–1.9 V vs. Li/Li^+ to avoid any side reactions or formation of new phases, and no peaks in entropy change were measured near 100% SOC, as shown in Fig. 4a. Lu et al. [34] attributed the small absolute value of the entropy change to the almost zero change in the unit cell parameters during the two-phase transition.

3.3. Special features and sources of error in the potentiometric measurements of half-cells

For most of the measurements only a tolerable shift of maximum 0.5 mV in the OCV was observed between the

measurements at +20 °C before and after the temperature ramp (Fig. 2). However, a slightly increasing OCV was observed at 1% SOC for both LMFP and LTO, and additionally at 50–90% SOCs for the LMFP material. At 1% SOC of LMFP and LTO, the OCV was continuously shifting to higher values, but the increase became emphasized during the +30 °C measurement. Inside the 50–90% SOC range in LMFP, an upward shift in the OCV value was observed only during the +30 °C measurement. The increase in OCV implies minor losses of lithium-ions from the LMFP and LTO electrode material lattices, which is accelerated at elevated temperatures. The impact of this was studied by determining the shift in OCV and using it for correcting the OCVs recorded at +30 °C. The shift was assumed to grow linearly during the +30 °C measurement and it was correspondingly subtracted from the measured values. Also the entropy change based on the measurement range of 0–+20 °C without the +30 °C measurement was determined. It was however observed that correcting for the OCV shift did not affect the calculated entropy change values significantly. Thus the entropy change values for these SOCs were calculated using all the measurement points 0–+30 °C without corrections. Nevertheless, the minor loss of lithium from LMFP in the Mn region suggests a somewhat more unstable structure compared to the Fe region, possibly also promoted by the higher potential of the Mn plateau. Indeed, minor Mn dissolution from LMFP materials at elevated temperatures has been observed [19,28].

Especially, near the transition point from Fe^{2+}/Fe^{3+} region to the Mn^{2+}/Mn^{3+} region of LMFP (at SOC = 32.5%) an unstable OCV behavior was observed, showing a clear and distinct downward drift of 3 mV. At 30% and 35% SOCs the same effect was seen but only in the tolerable order of 1 mV. As the OCV value decreases with time, the reason cannot be loss of lithium from the LMFP lattice, as that would lead to an increased OCV. Thus no correction to OCV due to loss of lithium was made. The unstable OCV behavior is attributed here to the transition from the Fe^{2+}/Fe^{3+} to the Mn^{2+}/Mn^{3+} redox reaction.

In LTO half-cells, the 5% and 10% SOC measurement points showed a hysteresis in the OCV vs. temperature behavior. Thus additional potentiometric measurements were conducted at 2%, 5% and 10% SOC over a wider temperature range (−10 °C to +25 °C) with OCV values recorded after every 5 °C temperature increment. Stabilization after the SOC adjustment was again performed at +20 °C for 20 h. The results are presented in Fig. 5, where an example of the measured OCV vs. temperature plots at 5% SOC is shown. The corresponding measurement at 2% SOC is shown in the inset for comparison. Linear fittings of the different regions are drawn as guides for eye. As the temperature is first increased (from −10 °C to +25 °C), it is observed in Fig. 5 that the slope of the OCV vs. temperature curve at 5% SOC is first positive, corresponding to a positive entropy change value, but then turns to negative, corresponding to a negative entropy change value. Similarly, when the temperatures are scanned back (from +25 °C to −10 °C), the slope is again first positive turning then to negative. The temperatures were also scanned in reverse order and using a doubled measurement time at each temperature (results not shown here), but the behavior corresponded to Fig. 5. When the same experiments were done at 10% SOC, a similar hysteresis was observed but it was less distinct. When the measurements at 2% and 5% SOC are compared, it is seen that the 2% SOC does not show any hysteresis but maintains the positive slope for the whole temperature range in both directions. Loss of lithium from the LTO lattice cannot have produced the change of the slope as it would have only caused a constant increase in the OCV values. In this study, the negative slope was taken to represent the entropy change at 5% and 10% SOC, according to the majority of measurement points. The entropy change value was calculated as average from repetition measurements, to minimize

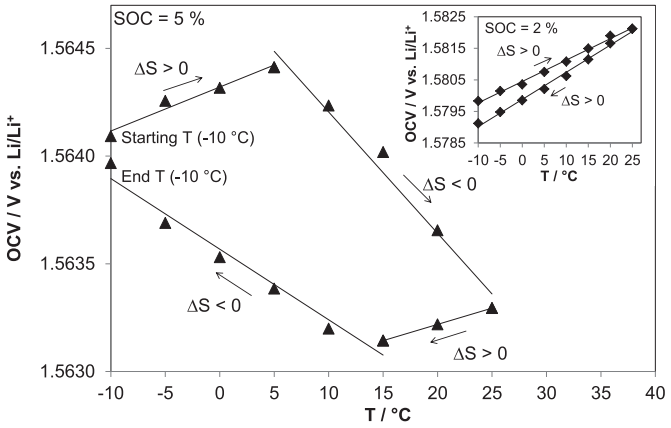

Fig. 5. OCV vs. temperature of the LTO half-cell at 5% SOC with temperatures scanned from −10 °C to +25 °C and back to −10 °C. Corresponding measurement at 2% SOC is shown in the inset.

the effect of possible slight inaccuracy in the SOC. Additionally, it is suggested by the voltage profile in Fig. 1b and proposed in literature [8] that the 5% and 10% SOC are already in the two-phase region similar to the higher SOCs, which show negative entropy change values. Based on these observations, it is speculated here that the 5–10% SOC range, although in the two-phase region, might show here residues of the possible solid-solution region (located near 0% SOC). This would have caused the distinct hysteresis in the OCV vs. temperature behavior at 5% and 10% SOC. Wagemaker et al. [51] proposed that the two-phase composition is unstable relaxing to solid-solution single phase, which could affect potentiometric measurements when relatively long stabilization and measurement times are used. However, the results of this study in Figs. 4a and 5 do not support this. The hysteresis phenomenon should be in any case studied more in detail to explain it reliably.

3.4. Comparison of full cell and half-cell entropy change results

The entropy change of an LMFP/LTO full cell was measured similarly to the half-cells. The measured values are compared with simulated entropy change values, calculated from the half-cell results according to Eq. (2). LTO/LMFP ratio of the full cell was 1.24, which is taken into account in the calculations. The comparison is shown in Fig. 6. The OCV value taken from the +20 °C measurement of the LMFP/LTO full cell is plotted for each SOC.

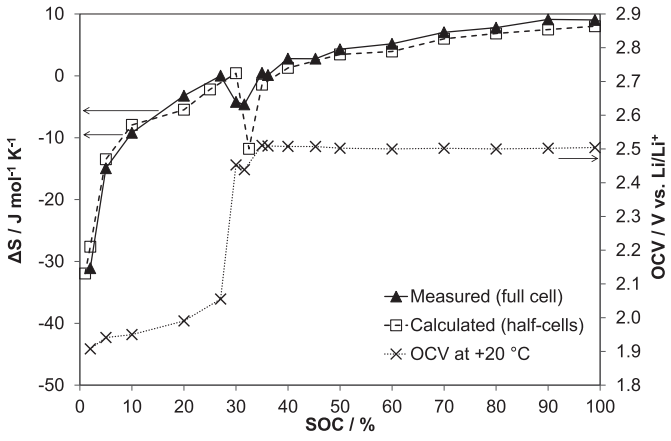

Fig. 6. Comparison of measured (full cell) and calculated (based on half-cell results) entropy change values. In addition, the OCV values at +20 °C for the full cell are plotted.

According to Fig. 6, the measured entropy change of an LMFP/LTO test cell corresponds well to the predicted, calculated values based on half-cell measurement data. Slight variation is seen in the absolute values, but the trend is very similar. It is also observed that there is a slight shift along the SOC-axis, which is due to the consumption of active lithium in side reactions, distorting the SOC values of the full cell to some extent. In half-cells, there is an infinite amount of lithium-ions but in full cells, all the active lithium is brought to the cell with the LMFP material and its amount is thus limited. This distortion of the SOC values is also seen as slight inconsistency between the adjacent entropy change and OCV values near 30% SOC. The result presented in Fig. 6 confirms the half-cell results and also shows that the use of lithium counter electrode has not interfered with the measured entropy change values. Also here in the full cell entropy change, a negative peak is observed at approximately 31% SOC. This corresponds to the negative entropy change peak observed for LMFP material at 32.5% SOC. At this point, an abrupt change in the +20 °C OCV value, characteristic for the Fe–Mn transition region, is observed, too.

3.5. Simulated entropy change of different electrode material combinations

To simulate the entropy change of different cell chemistries, half-cell results were utilized. The entropy change of a particular electrode combination was calculated according to Eq. (2) from the corresponding half-cell results. The calculated entropy changes for different combinations of LMFP or LFP positive electrodes and LTO or graphite negative electrodes are presented in Fig. 7. Negative/positive electrode ratios were taken to be 1. The data for LFP and graphite electrodes was taken from a previous study [29].

According to Fig. 7, the net entropy change would be closest to zero for a cell with an LFP positive and an LTO negative electrode (Fig. 7a). The entropy changes of LFP for reduction and LTO for oxidation are nearly equal in magnitude but opposite in sign, and thus they cancel each other out giving a net entropy change close to zero when these materials are combined in a cell. Thus for this combination, the variation in the cell's heat generation over the whole SOC range would be the smallest due to the smallest reversible heat generation rate. LMFP/LTO combination shows slightly more variation in entropy change as the beneficial effect of the positive and negative electrode entropy changes is smaller due to the almost net zero entropy change of the Mn region and the more negative and sloping entropy change of the Fe region. According to the study of Viswanathan et al. [32], cells with LCO positive electrode show significantly high absolute values of the net entropy change due to the large magnitude of the entropy change of LCO. Compared to this, the entropy change of LMFP is much smaller in magnitude, thus resulting in smaller net entropy change for LMFP based cells.

Cells containing a graphite negative electrode show a region of a clearly positive entropy change in the intermediate SOC range (Fig. 7b). This positive entropy change for the full cell is due to the graphite's stage-2L ↔ stage-2 – transition [29]. The positive entropy change leads to a cooling effect during discharge and respectively additional heat production during charge [29]. Combinations with LTO negative electrode do not have this feature, as the entropy change of LTO is almost constant when the SOCs close to 0% are not considered. This means that there is overall less heat variation for cells with LTO negative electrode. Lu et al. [34] compared the thermal behavior of cells consisting of LTO or mesocarbon-microbead (MCMB) graphite with $Li_{1.156}Mn_{1.844}O_4$ (LMO) positive electrode. They showed that the LTO negative electrode cell had a smaller and more constant entropy change, and thus also less heat variation in the cell. This is well consistent with the half-cell calculations of this study. Viswanathan et al. [32] also came to this conclusion.

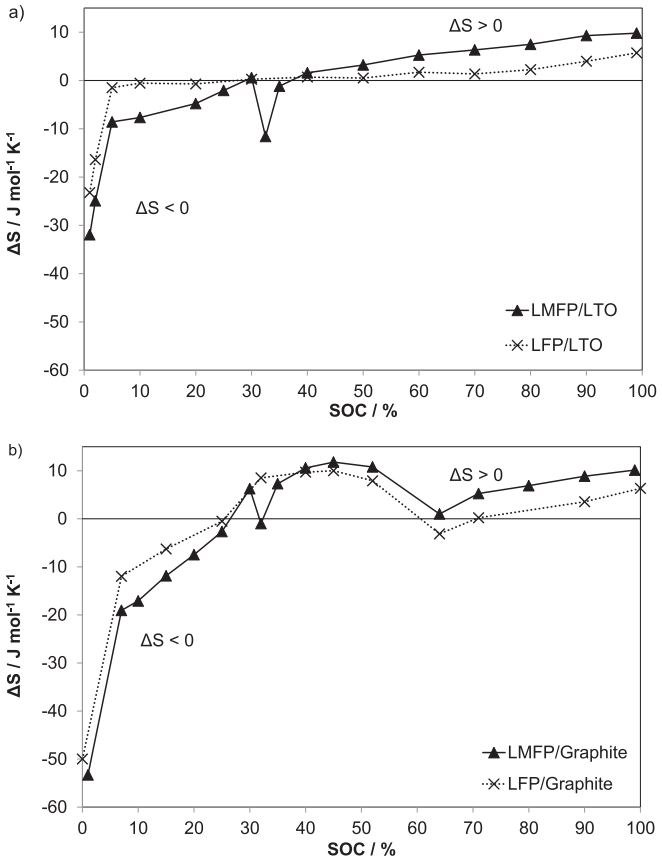

Fig. 7. Calculated entropy change for different combinations of LMFP or LFP positive and LTO or graphite negative electrodes based on half-cell measurements. Data for LFP and graphite is taken from a previous study [29]. (a) LMFP/LTO and LFP/LTO; (b) LMFP/graphite and LFP/graphite.

Inside the 0–10% SOC range, the entropy change is strongly negative for all combinations and especially for those with graphite negative electrode. This means that discharging the cells to empty evolves heat, as was already concluded for the LFP/graphite combination [29]. Thus extra thermal stress can be avoided it the cells are not discharged to completely empty, but always left to minimum of 10% SOC, for example.

4. Conclusions

In this work, the entropy change for LMFP ($LiMn_{0.67}Fe_{0.33}PO_4$) and LTO materials was determined as function of SOC, and the obtained values were compared to LFP and graphite from a previous study. Also the entropy change for cells of different electrode material combinations was simulated by using half-cell results.

For LMFP, the entropy change was found to follow the distinct redox reaction regions of Fe^{2+}/Fe^{3+} and Mn^{2+}/Mn^{3+}. The entropy change in Fe^{2+}/Fe^{3+} region is clearly affected by the addition of Mn to the olivine structure. The difference could be due to the changed mechanism of the Fe^{2+}/Fe^{3+} redox reaction, from the two-phase reaction in pure LFP to a single-phase solid-solution reaction in LMFP. The Mn^{2+}/Mn^{3+} region shows a rather constant entropy change behavior, resembling more a two-phase reaction at least at higher SOCs. Near the transition between Mn^{2+}/Mn^{3+} and Fe^{2+}/Fe^{3+} redox reactions, unstable OCV behavior and a sharp peak in the entropy change were observed, suggesting a single-phase

region existence. Further studies with concurrent phase diagram detection should be performed in order to conclude with unambiguity how the entropy change behavior reflects the two-phase versus single-phase mechanisms. As the Mn content of LMFP has been proposed to significantly affect the existence of single-phase regions, measurements on LMFP materials with various Mn contents should be conducted.

The entropy change of LTO showed a slightly negative and almost constant value inside the SOC range of 5–100%, typical of a two-phase reaction. In the 0–5% SOC range, a positive peak in entropy change was observed, which could be due to a single-phase solid solution region. The entropy change of LTO should still be studied further inside the 0–5% SOC range in terms of the possible single-phase existence.

The simulated entropy change values for different electrode material combinations were compared and LFP/LTO combination showed a net entropy change closest to zero. This was due to the beneficial effect of the individual entropy change values of LFP and LTO, which cancel each other out for the most part. The entropy change of LMFP, although close to zero for the Mn region, is slightly less beneficial. On the negative electrode side, cells with LTO show a smaller absolute net entropy change when compared to graphite.

All studied combinations have a notable, negative net entropy change in the SOCs of 0–10%. In practice this will lead to extra heat production during discharge inside this SOC range. For many applications, only a part of the entire 0–100% SOC range is utilized and by avoiding the 0–10% SOC range extra heat production and thus thermal stress could be diminished. Knowledge of the entropy change characteristics of new, promising electrode materials is important for predicting the cell thermal behavior and designing the battery cooling system.

The LMFP/LTO combination seems to be a very promising choice for large applications, as it is very safe and still able to provide a good energy density. In terms of cell's thermal behavior, an LMFP/LTO cell shows smaller absolute net entropy change and thus less reversible heat generation than LCO [32] or graphite based cells. LFP/LTO combination would be slightly more beneficial in terms of minimizing the reversible heat generation, but the cell voltage and thus the energy density can be substantially increased by using LMFP instead of LFP.

Acknowledgments

The authors greatly thank Clariant for providing electrode material powders.

References

[1] T. Ohzuku, A. Ueda, N. Yamamoto, J. Electrochem. Soc. 142 (1995) 1431–1435.
[2] K. Kanamura, H. Naito, Z.-I. Takehara, Chem. Lett. 1 (1997) 45–46.
[3] T. Ohzuku, A. Ueda, N. Yamamoto, Y. Iwakoshi, J. Power Sources 54 (1995) 99–102.
[4] E. Ferg, R.J. Gummow, A. de Kock, M.M. Thackeray, J. Electrochem. Soc. 141 (1994) L147–L150.
[5] K. Amine, I. Belharouak, Z. Chen, T. Tran, H. Yumoto, N. Ota, S.-T. Myung, Y.-K. Sun, Adv. Mater. 22 (2010) 3052–3057.
[6] S. Panero, P. Reale, F. Ronci, B. Scrosati, P. Perfetti, V.R. Albertini, Phys. Chem. Chem. Phys. 3 (2001) 845–847.
[7] K. Kanamura, T. Umegaki, H. Naito, Z. Takehara, T. Yao, J. Appl. Electrochem. 31 (2001) 73–78.
[8] S. Scharner, W. Weppner, P. Schmid-Beurmann, J. Electrochem. Soc. 146 (1999) 857–861.
[9] A. Yamada, S.C. Chung, K. Hinokuma, J. Electrochem. Soc. 148 (2001) A224–A229.
[10] H. Huang, S.-C. Yin, L.F. Nazar, Electrochem. Solid-State Lett. 4 (2001) A170–A172.
[11] A.K. Padhi, K.S. Nanjundaswamy, J.B. Goodenough, J. Electrochem. Soc. 144 (1997) 1188–1194.
[12] M. Yonemura, A. Yamada, Y. Takei, N. Sonoyama, R. Kanno, J. Electrochem. Soc. 151 (2004) A1352–A1356.
[13] C. Delacourt, L. Laffont, R. Bouchet, C. Wurm, J.-B. Leriche, M. Morcrette, J.-M. Tarascon, C. Masquelier, J. Electrochem. Soc. 152 (2005) A913–A921.
[14] A. Yamada, S.-C. Chung, J. Electrochem. Soc. 148 (2001) A960–A967.
[15] Z.X. Nie, C.Y. Ouyang, J.Z. Chen, Z.Y. Zhong, Y.L. Du, D.S. Liu, S.Q. Shi, M.S. Lei, Solid State Commun. 150 (2010) 40–44.
[16] A. Yamada, M. Hosoya, S.-C. Chung, Y. Kudo, K. Hinokuma, K.-Y. Liu, Y. Nishi, J. Power Sources 119–121 (2003) 232–238.
[17] J. Hong, F. Wang, X. Wang, J. Graetz, J. Power Sources 196 (2011) 3659–3663.
[18] A. Yamada, Y. Kudo, K.-Y. Liu, J. Electrochem. Soc. 148 (2001) A1153–A1158.
[19] V. Borgel, G. Gershinsky, T. Hu, M.G. Theivanayagam, D. Aurbach, J. Electrochem. Soc. 160 (2013) A650–A657.
[20] G. Li, H. Azuma, M. Tohda, J. Electrochem. Soc. 149 (2002) A743–A747.
[21] Q.-Q. Zou, G.-N. Zhu, Y.-Y. Xia, J. Power Sources 206 (2012) 222–229.
[22] G. Chen, T.J. Richardson, J. Power Sources 195 (2010) 1221–1224.
[23] G. Chen, T.J. Richardson, J. Electrochem. Soc. 156 (2009) A756–A762.
[24] S.-W. Kim, J. Kim, H. Gwon, K. Kang, J. Electrochem. Soc. 156 (2009) A635–A638.
[25] D. Strand, B. Gerhart, B. Landes, B. Kern, A. Pasztor, B. Nickless, A. Wallace, Ceram. Trans. 233 (2012) 101–115.
[26] S.K. Martha, O. Haik, E. Zinigrad, I. Exnar, T. Drezen, J.H. Miners, D. Aurbach, J. Electrochem. Soc. 158 (2011) A1115–A1122.
[27] S.K. Martha, E. Markevich, V. Burgel, G. Salitra, E. Zinigrad, B. Markovsky, H. Sclar, Z. Pramovich, O. Heik, D. Aurbach, I. Exnar, H. Buqa, T. Drezen, G. Semrau, M. Schmidt, D. Kovacheva, N. Saliyski, J. Power Sources 189 (2009) 288–296.
[28] A. Guéguen, L. Castro, R. Dedryvère, E. Dumont, J. Bréger, C. Tessier, D. Gonbeau, J. Electrochem. Soc. 160 (2013) A387–A393.
[29] K. Jalkanen, T. Aho, K. Vuorilehto, J. Power Sources 243 (2013) 354–360.
[30] D. Bernardi, E. Pawlikowski, J. Newman, J. Electrochem. Soc. 132 (1985) 5–12.
[31] R.E. Williford, V.V. Viswanathan, J.G. Zhang, J. Power Sources 189 (2009) 101–107.
[32] V.V. Viswanathan, D. Choi, D. Wang, S. Xu, S. Towne, R.E. Williford, J.-G. Zhang, J. Liu, Z. Yang, J. Power Sources 195 (2010) 3720–3729.
[33] A.J. Bard, L.R. Faulkner, Electrochemical Methods, Fundamentals and Applications, second ed., J. Wiley & Sons, New York, 2001, pp. 47–48.
[34] W. Lu, I. Belharouak, J. Liu, K. Amine, J. Power Sources 174 (2007) 673–677.
[35] J. Dodd, Phase Composition and Dynamical Studies of Lithium Iron Phosphate (Ph.D. thesis), California Institute of Technology, 2007, pp. 75–94.
[36] Y. Reynier, R. Yazami, B. Fultz, J. Power Sources 119–121 (2003) 850–855.
[37] Y. Reynier, R. Yazami, B. Fultz, J. Electrochem. Soc. 151 (2004) A422–A426.
[38] G. Kobayashi, A. Yamada, S.-I. Nishimura, R. Kanno, Y. Kobayashi, S. Seki, Y. Ohno, H. Miyashiro, J. Power Sources 189 (2009) 397–401.
[39] Z.-H. Wang, L.-X. Yuan, W.-X. Zhang, Y.-H. Huang, J. Alloy. Compd. 532 (2012) 25–30.
[40] A. Yamada, Y. Kudo, K.-Y. Liu, J. Electrochem. Soc. 148 (2001) A747–A754.
[41] T. Muraliganth, A. Manthiram, J. Phys. Chem. C 114 (2010) 15530–15540.
[42] N.N. Bramnik, K.G. Bramnik, K. Nikolowski, M. Hinterstein, C. Baehtz, H. Ehrenberg, Electrochem. Solid-State Lett. 8 (2005) A379–A381.
[43] K.-W. Nam, W.-S. Yoon, K. Zaghib, K.Y. Chung, X.-Q. Yang, Electrochem. Commun. 11 (2009) 2023–2026.
[44] R. Malik, F. Zhou, G. Ceder, Phys. Rev. B 79 (2009) 214201–214207.
[45] M.R. Roberts, G. Vitins, G. Denuault, J.R. Owen, J. Electrochem. Soc. 157 (2010) A381–A386.
[46] J. Molenda, W. Ojczyk, K. Świerczek, W. Zając, F. Krok, J. Dygas, R.-S. Liu, Solid State Ionics 177 (2006) 2617–2624.
[47] J. Molenda, W. Ojczyk, J. Marzec, J. Power Sources 174 (2007) 689–694.
[48] A.M. Hashambhoy, J.F. Whitacre, J. Electrochem. Soc. 158 (2011) A390–A395.
[49] R.B. Ravnsbæk, L. Xiang, W. Xing, O.J. Borkiewicz, K.M. Wiaderek, P. Gionet, K.W. Chapman, P.J. Chupas, Y.-M. Chiang, Nano Lett. 14 (2014) 1484–1491.
[50] A. Yamada, H. Koizumi, S.-I. Nishimura, N. Sonoyama, R. Kanno, M. Yonemura, T. Nakamura, Y. Kobayashi, Nat. Mater. 5 (2006) 357–360.
[51] M. Wagemaker, D.R. Simon, E.M. Kelder, J. Schoonman, C. Ringpfeil, U. Haake, D. Lützenkirchen-Hecht, R. Frahm, F.M. Mulder, Adv. Mater. 18 (2006) 3169–3173.
[52] C. Kim, N.S. Norberg, C.T. Alexander, R. Kostecki, J. Cabana, Adv. Funct. Mater. 23 (2013) 1214–1222.
[53] K.E. Thomas, J. Newman, J. Power Sources 119–121 (2003) 844–849.
[54] S. Bach, J.P. Pereira-Ramos, N. Baffier, R. Messina, J. Electrochem. Soc. 138 (1990) 1042–1048.